J Mater Sci: Mater Med (2007) 18:103–109
DOI 10.1007/s10856-006-0667-8

On the measurement of human osteosarcoma cell elastic modulus using shear assay experiments

Yifang Cao · Randy Bly · Will Moore · Zhan Gao · Alberto M. Cuitino · Wole Soboyejo

Received: 20 October 2005 / Accepted: 28 February 2006

Abstract This paper presents a method for determining the elastic modulus of human osteosarcoma (HOS) cells. The method involves a combination of shear assay experiments and finite element analysis. Following in-situ observations of cell deformation during shear assay experiments, a digital image correlation (DIC) technique was used to determine the local displacement and strain fields. Finite element analysis was then used to determine the Young's moduli of HOS cells. This involved a match of the maximum shear stresses estimated from the experimental shear assay measurements and those calculated from finite element simulations.

1 Introduction

The understanding the biological responses of bone cells to mechanical loading has been a subject of interest in bioengineering and sciences [1–3]. One of the major mechanical stimuli that bone cells (osteoblasts and osteocytes) respond to is the deformation-generated fluid shear stress exerted by the insterstitial fluid flow through the lacunar/canalicular spaces [1, 3]. Shear assay experiments using a parallel-plate flow chamber have been used to study the in vitro behavior of osteoblast-like cells subjected to shear flow [1–6]. Prior studies have used the shear assay technique to explore fluid flow shear stress-induced deformation [4], biochemical changes [2], cell proliferation and differentiation [1, 5]. However, we are unaware of any prior experimental shear assay studies trying to relate the discrete nature of cell deformation to cell elastic properties.

The characterization of bone cell mechanical properties, especially their deformability, are crucial in the understanding and simulation of the bone adaption to mechanical stimuli [7]. The deformability of cells can be quantified by an effective elastic modulus. This is determined largely by the cell cytoskeleton, which consists largely of networks of microtubules, actin and intermediate filaments [8, 9]. The mechanical deformation of bone cells subject to a fluid flow shear stress is determined by the cell mechanical properties. It is also worthwhile to explore an inverse approach, in which the effective elastic modulus of bone cells can be determined using the deformation contour obtained in a shear assay experiment.

In this paper, the effective elastic moduli of human osteosarcoma (HOS) cells were determined using a combination of shear assay experiments and finite element analysis. Following an experimental study in which an in situ digital camera was used to examine cell deformation in shear assay experiments, the digital image correlation (DIC) technique [10] was used to determine the displacement and strain fields associated with the captured images. Finite element modeling was then used to determine the cell mechanical properties. The modeling involved the matching of the wall shear stresses, which were estimated from the shear assay experimental measurements and the shear stresses calculated from finite element simulations. The resulting average elastic moduli were in good agreement with recent results reported by Shin and Athanasiou [11] for osteoblasts.

Y. Cao · R. Bly · W. Moore · W. Soboyejo (✉)
Princeton Institute for the Science and Technology of Materials (PRISM) and Department of Mechanical and Aerospace Engineering, Princeton University, Princeton, NJ 08544
e-mail: soboyejo@princeton.edu

Z. Gao · A. M. Cuitino
Department of Mechanical and Aerospace Engineering, Rutgers University, Piscataway, NJ 08854

2 Experimental methods

2.1 Cell culture

Human osteosarcoma (HOS) cells (cultured from a frozen cell line obtained from ATCC, Manassas, VA) were cultured in 25 cm^2 medium-filled flasks (Becton-Dickinson, Franklin Lakes, NJ). The cells were kept in an incubator containing 5% CO_2, 95% air, saturated humidity, and held at a constant temperature of 37°C. A Dulbeccos Modified Eagle's Medium (DMEM) supplemented with 10% Fetal Bovine Serum (FBS) and 1% penicillin/streptomycin/amphotericin B was used as the cell culture medium (Quality Biological, Gaithersburg, MD). At confluence, the cells were harvested using 0.25% trypsin (sub-cultured by splitting). The cells were then seeded on polished Ti-6Al-4V ELI (Titanium Industries, Parsippany, NJ) substrates contained in polystyrene dishes. Afterwards, the cells were placed in an incubator for 48 h, before performing the shear assay experiments. The cells were seeded initially in serum free Dulbecco's Modified Eagle's Medium ($DMEM^-$). This allowed the cells to attach to the surface without the presence of artificial proteins that are usually found in the cell media. After two hours, the media was replaced with DMEM, supplemented with 10% Fetal Bovine Serum and 1% penicillin/streptomycin/amphotericin B ($DMEM^+$). This $DMEM^+$ contained nutrients required for the cells to live for longer than two hours.

2.2 Shear assay experiments

A shear assay system was used to measure the interfacial shear strength. This involved a laminar flow of a viscous fluid through a parallel plate flow chamber. An in-situ optical microscope was used to observe individual cells being deformed under shear flow. The shear assay experimental set-up and flow chamber are shown in Fig. 1. The parallel plate flow chamber (Glycotech Corporation, Rockville, MD) was designed to work on polystyrene dishes that have a 35.0 mm inner diameter. The apparatus has an outer diameter of 33.5 mm. The flow chamber dimensions are determined by the size of the gasket used. The gasket used in the present study had a chamber measuring 2.5 mm width × 20.5 mm length × 0.254 mm height. The gasket was attached to the substrate by a vacuum seal.

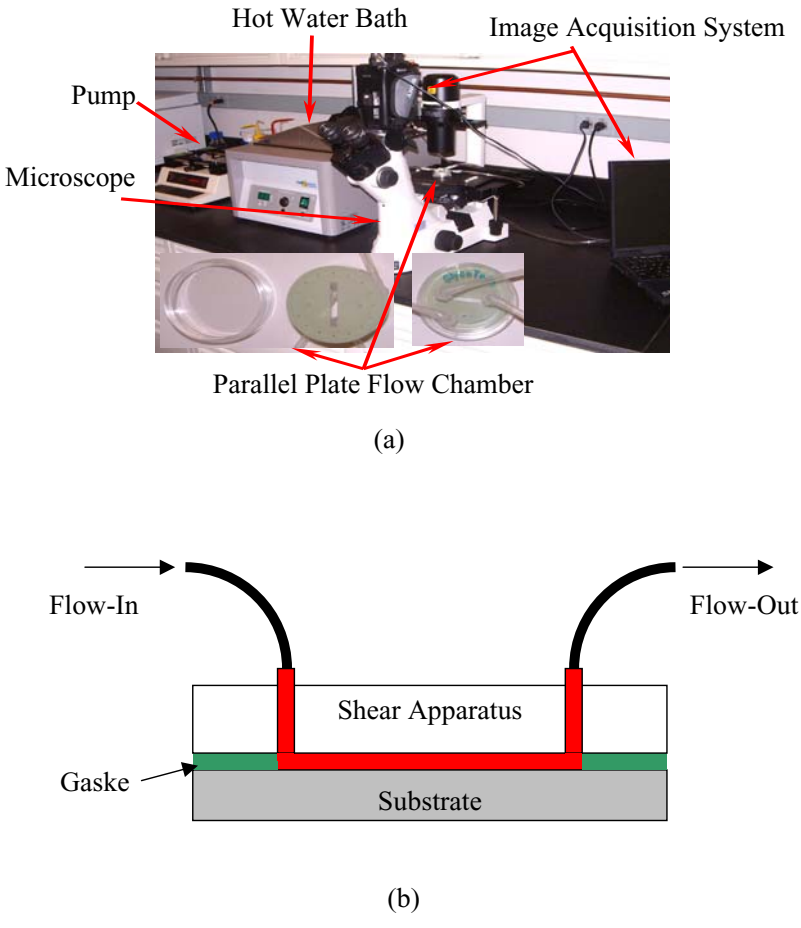

Fig. 1 (a) Shear assay experimental setup and flow chamber; (b) Cross-section of shear assay setup

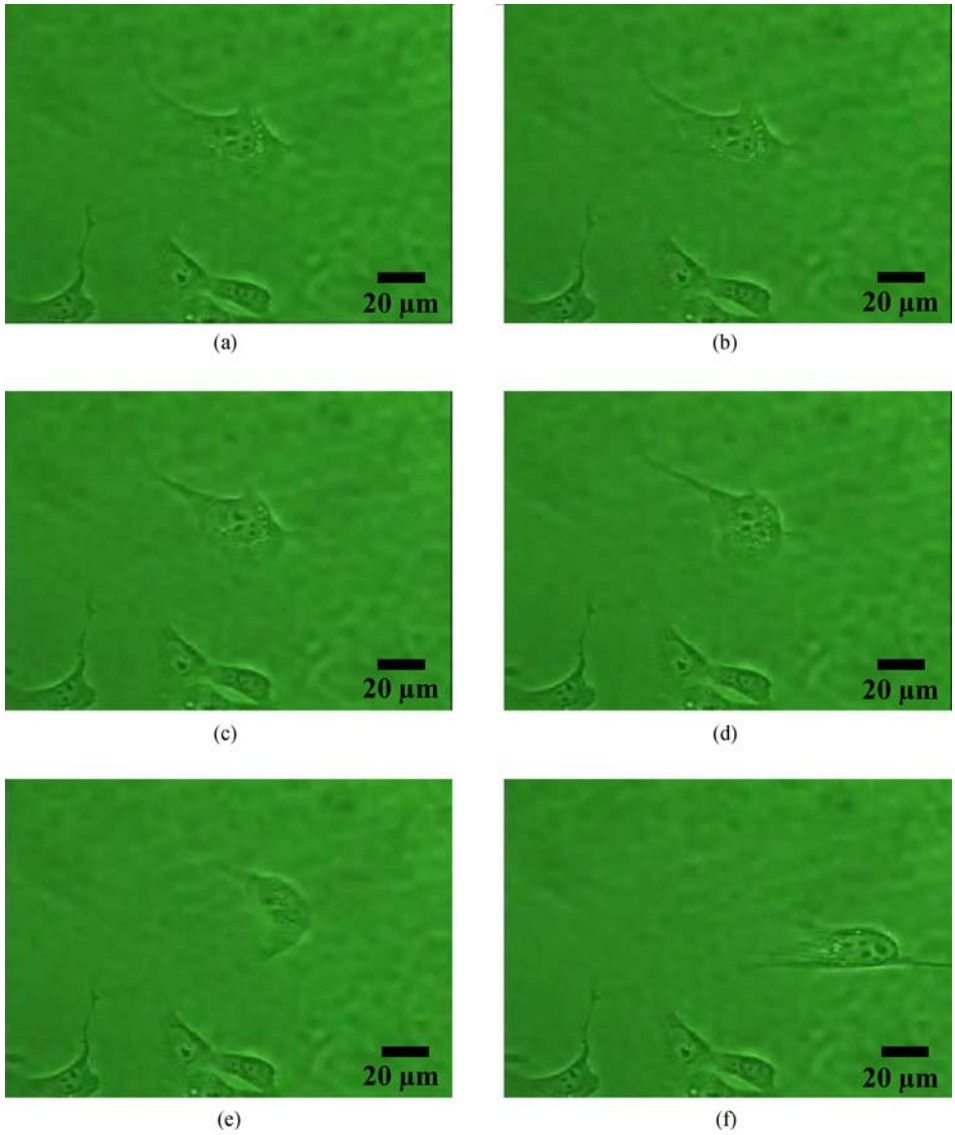

Fig. 2 Typical image sequences captured after the onset of flow during an shear assay experiment with the calculated wall shear stress of 70 Pa. (a) $t = 0$ s; (b) $t = 1.19$ s; (c) $t = 2.38$ s; (d) $t = 3.57$ s; (e) $t = 3.64$ s; (f) $t = 3.85$ s

A viscous flow medium of 60% methyl cellulose and 40% DMEM$^-$ (viscosity $= 3.34 \times 10^{-2}$ kg/ms) was used. This kept the flow rates (25 mL/hr to 500 mL/hr) and the Reynolds number to a minimum, thus permitting laminar flow. The images were captured using a CCD video camera, and a desktop computer. Typical image sequences captured during a shear assay experiment are shown in Fig. 2. The wall shear stress at the wall of the flow chamber τ_{wall} was determined from [6, 12, 13]:

$$\tau_{\text{wall}} = \frac{6\mu Q}{wh^2} \tag{1}$$

where Q represents the volumetric flow rate, μ represents the media viscosity, w and h are the width and height of the chamber, respectively.

3 Modeling

3.1 Digital image correlation technique

Digital Image Correlation (DIC) [10] can be effectively utilized to characterize the cell deformation pattern by sequential correlating the images recorded during the shear assay test. The cell can be clearly distinguished at the center of the images (Fig. 3). It is shown as a semi-transparent region filled with dark and bright dots. These speckles provide the necessary image texture for a successful image correlation using a Global Digital Image Correlation (GDIC) approach. In this technique a Lagrangian tracking of the material is enforced by following a virtually over-imposed mesh on the region of interest (in this case the cell) between two subsequent images. The deformation mapping between these

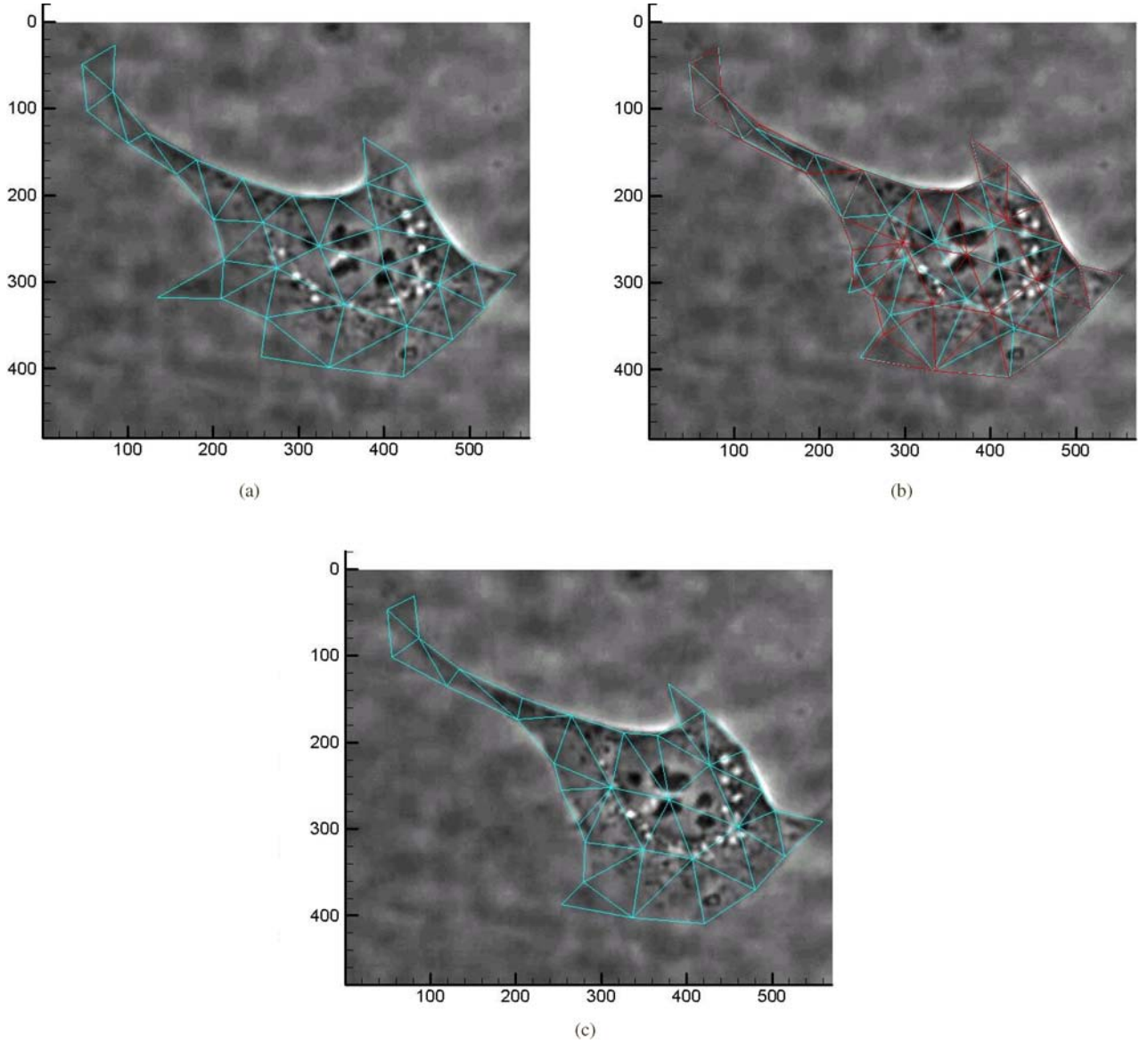

Fig. 3 Mesh superimposed on cell images. (a) The first undeformed cell and mesh; (b) Because one triangle element has been shrunk dramatically, a new mesh (red) was generated within the boundary; (c) The final image and computed mesh

two images is obtained by a multi-variable minimization which conducted on a constrained system determined by the mesh.

The initial triangular mesh, which tiles the entire cell, is shown in Fig. 3(a). Due to the severe deformations experienced by the cell during the assay test, a remeshing step is required to preserve the mesh quality and thus avoiding the associate problems of accuracy loss and lack of convergence. The remeshing step is indicated in Fig. 3(b). The final deformation state for which the stress state is computed is shown in Fig. 3(c). It should be noted that GDIC presents some advantages over the conventional or local DIC for this case. Mostly due to the fact that the fuzzy cell boundary makes one small portion of boundary on a local correlation window often indistinguishable from the others.

3.2 Finite element analysis

A finite element model was used to calculate the deformation and stress states of the cell. Cell deformation was analyzed using prior described digital image correlation technique. The DIC analysis was used to analyze the in-situ image sequences that were recorded during the shear assay experiments.

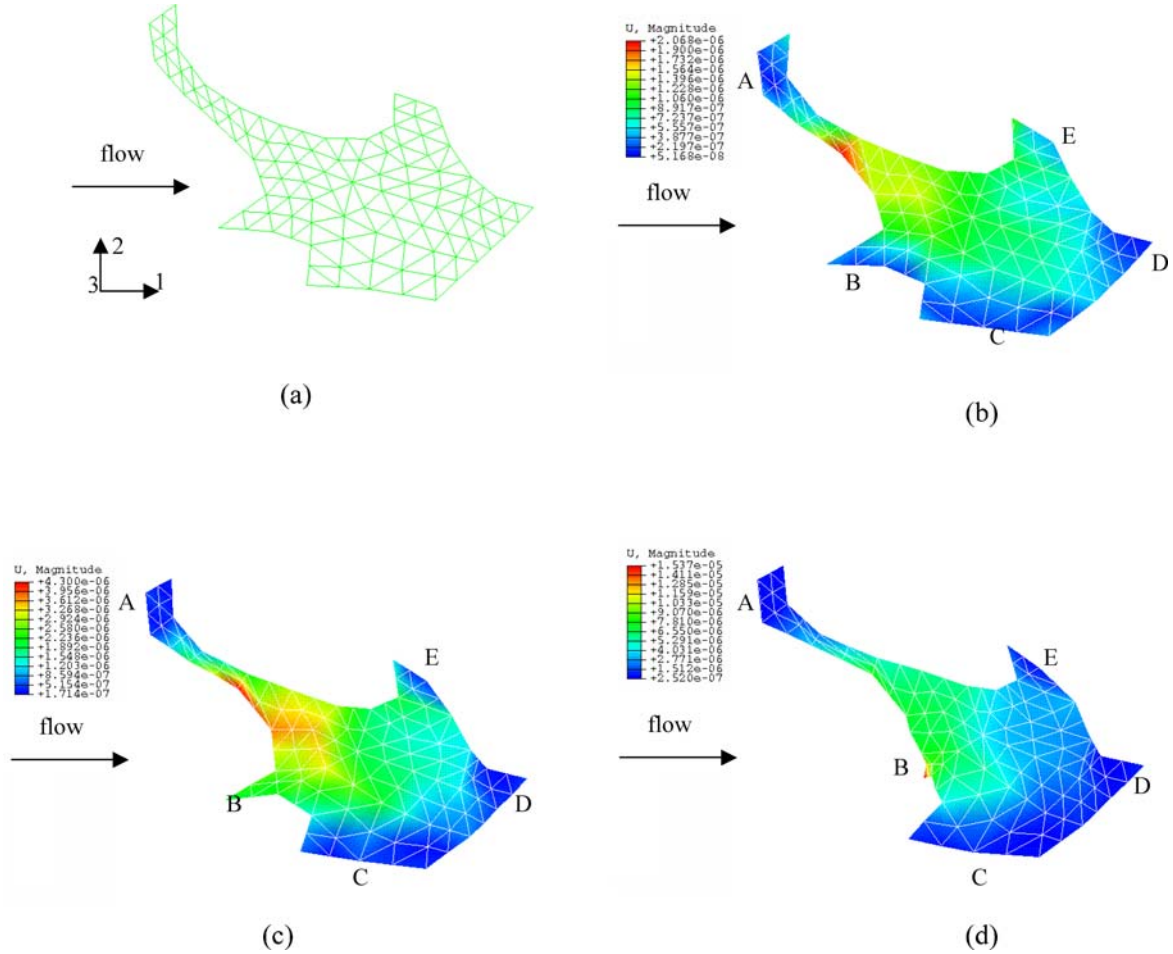

Fig. 4 The obtained displacement fields using the digital image correlation technique for the cell images captured in the shear assay experiment. The superimposed mesh is shown in (a); the deformation contours shown in (b), (c) and (d) are for $t = 1.19$ s, 2.38 s; and $t = 3.57$ s, respectively

The element strain vector ϵ was calculated using the element local nodal displacements $\hat{\mathbf{u}}$ through:

$$\epsilon = \mathbf{B}\hat{\mathbf{u}} \tag{2}$$

where $\mathbf{B}$ is the strain-displacement matrix [14]. The element stress vector τ was then calculated through:

$$\tau = \mathbf{C}\epsilon \tag{3}$$

where $\mathbf{C}$ is the material elasticity matrix which is only dependent on the elastic modulus E and Poisson's ratio ν for isotropic elasticity [14], which was assumed in the current study. Then finite element modeling [14] of the object leads to:

$$\mathbf{KU} = \mathbf{F} \tag{4}$$

where $\mathbf{U}$ and $\mathbf{F}$ are the vectors of nodal displacements and applied force, respectively; $\mathbf{K}$ is the stiffness matrix of the element assemblage, which is given by:

$$\mathbf{K} = \sum_m \mathbf{K}^{(m)} = \sum_m \int_{V^{(m)}} \mathbf{B}^{(m)\mathbf{T}} \mathbf{C}^{(m)} \mathbf{B}^{(m)} dV^{(m)} \tag{5}$$

Therefore, the stress distribution in cells subjected to shear deformation can be obtained using finite element simulations, when the material elasticity matrix $\mathbf{C}$ is given. The maximum shear stress at the onset of cell detachment can then be considered as a measure of interfacial strengths. This is usually around three times the wall shear stress [6, 12, 13, 15]. Hence, the effective Young's modulus of the cell can be estimated by matching the calculated maximum shear stress to three times of the measured wall shear stress. The ABAQUS (HKS Inc., Pawtucket, RI) software package was used to implement the finite element model. Triangular plane stress elements were used. The cells were assumed to be isotropic, linear elastic, and near incompressible [6, 7, 16]. The measured displacement fields obtained using the DIC technique, were prescribed as displacement boundaries in the simulations. Large displacement theory was used in the simulation

to fully account for the geometric nonlinearities in cell deformation, as in Ref. [6].

4 Results and discussion

The image sequences captured during a shear assay experiment (Fig. 2) show that the cell deformed in response to the applied shear flow, and finally, peeled off from the substrate and flipped over. The wall shear stress was calculated to be 70 Pa. Although the cell experienced significant deformation, when subjected to shear flow for several seconds, the initial deformation within the first second was not very significant.

The superimposed mesh for the plotting the DIC analysis results, and later the finite element analysis, is shown in Fig. 4(a). The displacement fields obtained using the DIC technique are shown in Figs. 4(b)–(d). These correspond to the deformed digital images shown in Figs. 2(b)–(d), respectively. When the cell was subjected to initial shear flow ($t = 1.19$ s, Fig. 2(b)), there were some regions (A, B, C, and D) in which the displacements were very small (with magnitudes of ∼100 nm). Such regions correspond to the focal adhesion (FA) sites [17].

However, the attachment of these focal point adhesions was weakened during the shear assay procedure, since the overall displacement increased with increasing time Figs. 4(b)–(d). Note that the attachment of these focal adhesion sites was not weakened uniformly, since the regions with smallest displacements gradually changed from region A, B, C, D at $t = 1.19$ sec, to region A, C, D, E at $t = 3.57$ sec (Figs. 4(b)–(d)). This may indicate the immobility of region B was weakened more than that in regions A, C and D, and region E was the least weakened. At $t = 3.57$ sec, the rear edge of the cell (region B) exhibited greater displacement with respect to the front edge (region E). This is consistent to prior cell motility studies in Ref. [18], in which higher mobility was observed at the rear edge, compared to the front edge subjected to shear flow. These cell responses to shear flow are actually associated with changes in the cytoskeleton that may include actin microfilament depolymerization and stress fiber alignment [17, 18]. Since cell elasticity is largely determined by the cytoskeleton [8], we will only focus on the initial deformation of the cell subjected to the shear flow, in which the change of cell cytoskeleton can be assumed to be small.

We only focus on the first second after the onset of the flow, which is much less than the cell relaxation time (above 60 sec) [19]. Although biological cells are essentially viscoelastic [8, 9], the cell should behave elastically in this early deformation regime.

The shear stress distribution in the cell is presented in Fig. 5. The maximum shear stress occurred at the rear edge of the cell, but close to the focal adhesion site A. Figure 6

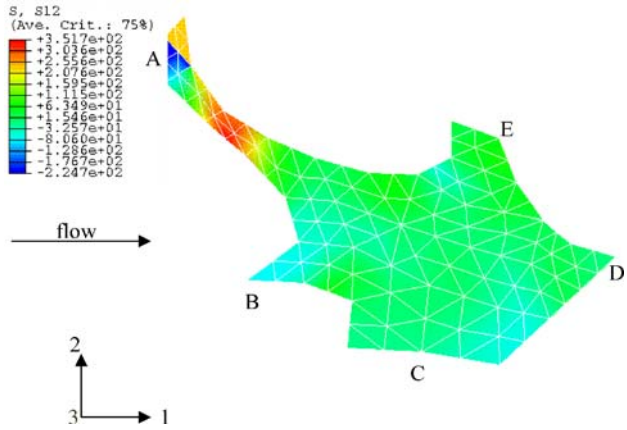

Fig. 5 The shear stress distribution of a cell subject to shear flow ($\tau_{wall} = 70$ Pa, $E = 3$ kPa, $\nu = 0.4$)

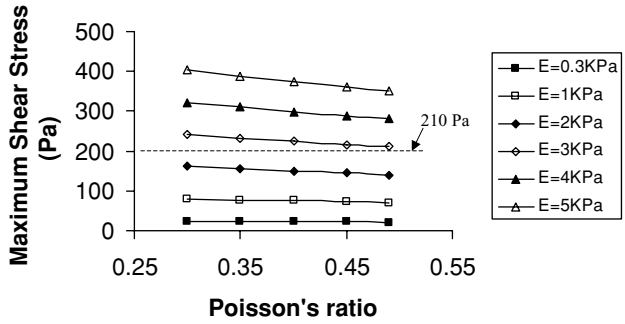

Fig. 6 The maximum shear stress calculated within the cell versus the Poisson's ratio for different cell moduli

shows the maximum shear stress calculated within the cell. This is plotted against the Poisson's ratio for different cell moduli. The results suggest that the Poisson's ratio does not have a significant effect on the maximum shear stress. This is true for Poisson's ratios close to the incompressibility condition, which is typical of most biological cells [6, 7, 16]. Furthermore, as the cell modulus increased, the maximum shear stress increased significantly. Also, the calculated maximum shear stresses were comparable to those reported in prior studies [6, 12, 13, 15], in which the maximum shear stresses were around three times the wall shear stresses. Considering that the applied wall shear stress is 70 Pa, the HOS cell effective modulus can be estimated to be 2–3 kPa. This is comparable to the effective modulus of 2 kPa measured for MG63 osteoblast-like cells in Ref. [11].

5 Conclusions

This paper presents a shear assay method for determining the elastic modulus of human osteosarcoma cells. The method involves digital image correlation and finite element analysis. The cell focal adhesions (along the cell front and rear edges) were found to change when the cell was subjected to shear

flow. An effective Young's modulus of 2–3 kPa was obtained from the combination of shear assay experiments and finite element simulations. This is in good agreement with prior results from osteoblask like MG63 cells, which have been shown to have Young's moduli of 2.05 ± 0.89 kPa.

Acknowledgments This work was supported by the National Science Foundation (Grant No.: DMR 0213706 and Grant No.: DMR 0231418). The authors are grateful to the NSF Program Manager, Dr. Carmen Huber, for her encouragement and support.

References

1. S. KAPUR, D. J. BAYLINK and K. W. LAU, *Bone* **32** (2003) 241.
2. E. A. NAUMAN, R. L. SATCHER, T. M. KEAVENY, B. P. HALLORAN and D. D. BIKLE, *J. Appl. Physiol.* **90** (2001) 1849.
3. V. I. SIKAVITSAS, J. S. TEMENO and A. G. MIKOS, *Biomaterials.* **22** (2001) 2581.
4. J. G. MCGARRY, J. KLEIN-NULEND, M. G. MULLENDER and P. J. PRENDERGAST, *Faseb J.* **18** (2004) 1.
5. U. LIEGIBEL, U. SOMMER, B. BUNDSCHUH, B. SCHWEIZER, U. HISCHER, A. LIEDER, P. NAWROTH and C. KASPERK, *Exper. Clin. Endocrinol. Diab.* **112** (2004) 356.
6. X. E. GUO, E. TAKAI, K. LIU and X. WANG, in Proceedings of 2001 ASME International Mechanical Engineering Congress and Exposition (New York, NY, Nov. 2001), BED-23160 p. 1.
7. G. T. CHARRAS and M. A. HORTON, *Biophys. J.* **83** (2002) 858.
8. G. BAO and S. SURESH, *Nature Mater.* **2** (2003) 715.
9. C. ZHU, G. BAO and N. WANG, *Annu. Rev. Biomed. Eng.* **2** (2000) 189.
10. Y. WANG and A. M. CUITINO, *Int. J. Sol. Struct.* **39** (2002) 3777.
11. D. SHIN and K. ATHANASIOU, *J. Orthop. Res.* **17** (1999) 880.
12. J. CAO, B. DONELL, D. R. DEAVER, M. B. LAWRENCE and C. DONG, *Microv. Res.* **55** (1998) 124.
13. S. B. BROOKS and A. TOZEREN, *Comp. Fluids* **25** (1996) 741.
14. K.-J. BATHE, in "Finite Element Procedures" (Prentice Hall, Englewood Cliffs, New Jersey, 2003).
15. C. DONG and X. X. LEI, *J. Biomech.* **33** (2000) 35.
16. T. OHASHI, Y. ISHII, Y. ISHIKAWA, T. MATSUMOTO and M. SATO, *Bio-Medical Mater. Eng.* **12** (2002) 319.
17. G. GIVELEKOGLU-SCHOLEY, A. W. ORR, I. NOVAK, J. J. MEISTER, M. A. SCHWARTZ and A. MOGILNER, *J. Theor. Biol.* **232** (2005) 569.
18. E. DECAVE, D. RIEU, J. DALOUS, S. FACHE, Y. BRECHET, B. FOURCADE, M. SATRE and F. BRUCKERT, *J. Cell Sci.* **116** (2003) 4331.
19. C. M. LO and J. FERRIER, *Eur. Biophys. J.* **28** (1999) 112.